Tetramerization of the S100B Chaperone Spawns a Ca^{2+} Independent Regulatory Surface that Enhances Anti-aggregation Activity and Client Specificity

António J. Figueira [1,2], Guilherme G. Moreira [1,2], Joana Saavedra [3,4,5], Isabel Cardoso [3,4,5] and Cláudio M. Gomes [1,2]*

*1 - **BioISI – Instituto de Biosistemas e Ciências Integrativas,** Faculdade de Ciências, Universidade de Lisboa, 1749-016 Lisboa, Portugal*
*2 - **Departamento de Química e Bioquímica,** Faculdade de Ciências, Universidade de Lisboa, 1749-016 Lisboa, Portugal*
*3 - **i3S – Instituto de Investigação e Inovação em Saúde,** Universidade do Porto, Porto, Portugal*
*4 - **IBMC - Instituto de Biologia Molecular e Celular,** Universidade do Porto, Porto, Portugal*
*5 - **ICBAS – Instituto de Ciências Biomédicas Abel Salazar,** Universidade do Porto, Portugal*

Correspondence to Cláudio M. Gomes: BioISI – Instituto de Biosistemas e Ciências Integrativas, Faculdade de Ciências, Universidade de Lisboa, 1749-016 Lisboa, Portugal. *cmgomes@fc.ul.pt (C.M. Gomes) @Antonio27902425 (A.J. Figueira), @GuilhermeGilMo1 (G.G. Moreira), @ClaudioGomesLab (C.M. Gomes)*
https://doi.org/10.1016/j.jmb.2022.167791
Edited by Louise C. Serpell

Abstract

Alzheimer's disease (AD) hallmarks include the aggregation of amyloid-β (Aβ), tau and neuroinflammation promoted by several alarmins. Among these is S100B, a small astrocytic homodimeric protein, upregulated in AD, whose multiple biological activities depend on localization, concentration, and assembly state. S100B was reported to inhibit the aggregation and toxicity of Aβ42 and tau similarly to a holdase-type chaperone. This activity is dependent of Ca^{2+}-binding, which triggers the exposure of a regulatory binding cleft at the S100B dimer interface with which amyloidogenic clients dynamically interact. Although the dimer prevails, a significant portion of secreted S100B in the human brain occurs as higher order multimers, whose protective functions remain uncharacterized and which we here investigate. Resorting to ThT-monitored aggregation kinetics, we determined that unlike the dimer, tetrameric S100B inhibits Aβ42 aggregation at sub/equimolar ratios, an effect that persists in the absence of Ca^{2+} binding. Structural analysis revealed that S100B tetramerization spawns a novel extended cleft accommodating an aggregation-prone surface that mediates interactions with monomeric Aβ client via hydrophobic interactions, as corroborated by Bis-ANS fluorescence and docking analysis. Correspondingly, at high ionic strength that reduces solvation and favours hydrophobic contacts, the inhibition of Aβ42 aggregation by tetrameric S100B is 3-fold increased. Interestingly, this extended Ca^{2+}-independent surface favours Aβ42 as substrate, as tau K18 aggregation is not inhibited by the apo tetramer. Overall, results illustrate a mechanism through which oligomerization of the S100B chaperone fine-tunes anti-aggregation activity and client specificity, highlighting the potential functional relevance of S100B multimers in the regulation of AD proteotoxicity.

Introduction

Proteotoxic insults caused by aggregation of the amyloid-β peptide (Aβ) into extracellular senile plaques and hyperphosphorylated tau into neurofibrillary tangles are major hallmarks of Alzheimer's disease (AD).[1] Nevertheless, other biochemical processes are altered in AD brain,

including sustained neuroinflammation promoted by several pro-inflammatory alarmins[2–3].

The small homodimeric (2 × 10.7 kDa) Ca^{2+}-binding S100B protein, which is often upregulated in AD,[4] is one such alarmin. In the brain, this multifunctional protein exerts both neurotrophic and deleterious effects, in a concentration and localization dependent fashion.[5–6] Under physiological conditions, S100B stimulates neurite growth[7] and plays several housekeeping functions.[8] However, in neurodegenerative contexts such as AD late stages, upregulated S100B is secreted by astrocytes into the synaptic milieu, promoting neuroinflammation through activation of the receptor for advanced glycation end products (RAGE),[6,9] which ultimately engages the nuclear translocation of the pro-inflammatory NF-κB transcription factor.[10] Despite this, neuroprotective functions for S100B have been unveiled, which imply S100 alarmins in vital housekeeping processes that harness early stages of AD, including chaperone activities.[5,11] Recently, we showed that S100B suppresses Aβ42[12] and tau[13] aggregation and toxicity by acting as a holdase-type chaperone and metal ion buffering protein.[14–16] Such chaperone activities result of dynamic protein–protein interactions established between S100B and Aβ42/tau monomers, oligomers and fibrils. In particular, nuclear magnetic resonance (NMR), small-angle X-ray scattering (SAXS) and computational predictions revealed that interaction with monomeric Aβ42 and tau is mainly driven by residues belonging to S100B hydrophobic dimer interfacial cleft and neighbouring regions,[12–13,17] whose solvent exposure is dependent of Ca^{2+} binding to the four EF-hand domains[18].

Consistent with a wide landscape of functions, many members of the S100 protein family are found in diverse homo- and hetero- oligomerization states,[19–22] such as the S100A12 dimer and hexamer,[23] the S100A8/A9 heterodimer and heterotetramer[24] or the S100A4 decamer.[25] Indeed, dimeric S100B also self-assembles into high order multimers, such as tetramers, hexamers and octamers, which are held together by non-covalent contacts.[26–27] The structures of homo-tetrameric and homo-octameric S100B were previously resolved by X-ray crystallography, suggesting the involvement of amino acid residues from S100B N-terminal (helix I) and C-terminal (helix IV) regions for complex stabilization.[28] S100B oligomers were also identified in human brain extracts,[28] where they seem to be tied with important roles underlying S100B pro-inflammatory signalling. It was observed that tetrameric S100B promotes RAGE dimerization and activation by interacting with receptor V domains with higher affinity than S100B homodimer.[26] Nonetheless, the impact of quaternary structure over S100B chaperone properties and specificity for client recognition, a factor which well known to be relevant in other chaperones[29–31] and for covalent disulfide cross linked S100B multimers[15], remains elusive and is here investigated.

Results and Discussion

Isolation of recombinant tetrameric S100B

Recombinant expression and purification of human S100B yields mostly S100B dimers but also minor populations of higher order homo-oligomers, including octamers, hexamers and tetramers[28,32] of which the latter are the predominant species. Thus, for this study, we have isolated highly pure S100B tetramers for comparative assays versus S100B dimers, which constitute the two most abundant S100B oligomers found *in vivo* and whose stability is independent of Ca^{2+} binding.[26] We have biochemically characterized and validated the purified S100B tetramers combining size-exclusion chromatography and electrophoretic analysis, under reducing and non-reducing conditions, and confirmed that the quaternary structure of these conformers is exclusively maintained by non-covalent interactions. Also, we have employed far-UV Circular Dichroism spectroscopy to establish that the S100B tetramer retains the typical α-helical topology of S100 proteins, similarly to the S100B dimer (Supplementary Figure 1).

Tetrameric S100B has enhanced anti Aβ42 aggregation activity

Next, we set out to compare the effect of the S100B tetramer versus that of the S100B dimer on the aggregation of Aβ42, in the presence of Ca^{2+}. To do so, we performed thioflavin-T (ThT) monitored aggregation kinetics using strictly monomeric Aβ42 preparations that yield aggregation profiles comparable to the best standards in the literature (Figure 1). In all assays, we tested the concentration of each S100B oligomer at the same quantity expressed in terms of dimer equivalents, or S100B total mass. As previously described, excess of dimeric S100B-Ca^{2+} inhibits Aβ42 aggregation but has a negligible effect at sub or equimolar ratios (Figure 1(**a**)), as inferred from effects in aggregation half-times ($t_{1/2}$) and ThT fluorescence amplitudes (Figure 1(**c**), (**d**)). Contrastingly, with tetrameric S100B-Ca^{2+} (Figure 1(**b**)) we observed a decrease on ThT amplitude even at sub stoichiometric ratios, suggesting a reduction of the final Aβ42 fibrillar mass content. Moreover, we noted that, at higher molar ratios, the S100B-Ca^{2+} tetramer drastically reduced the end point ThT fluorescence, practically abolishing Aβ42 fibrillation; likewise, the aggregation half-time increased even more than with dimeric S100B-Ca^{2+} (Figure 1(**c**), (**d**)).

We next employed transmission electron microscopy (TEM) to assess the morphology of

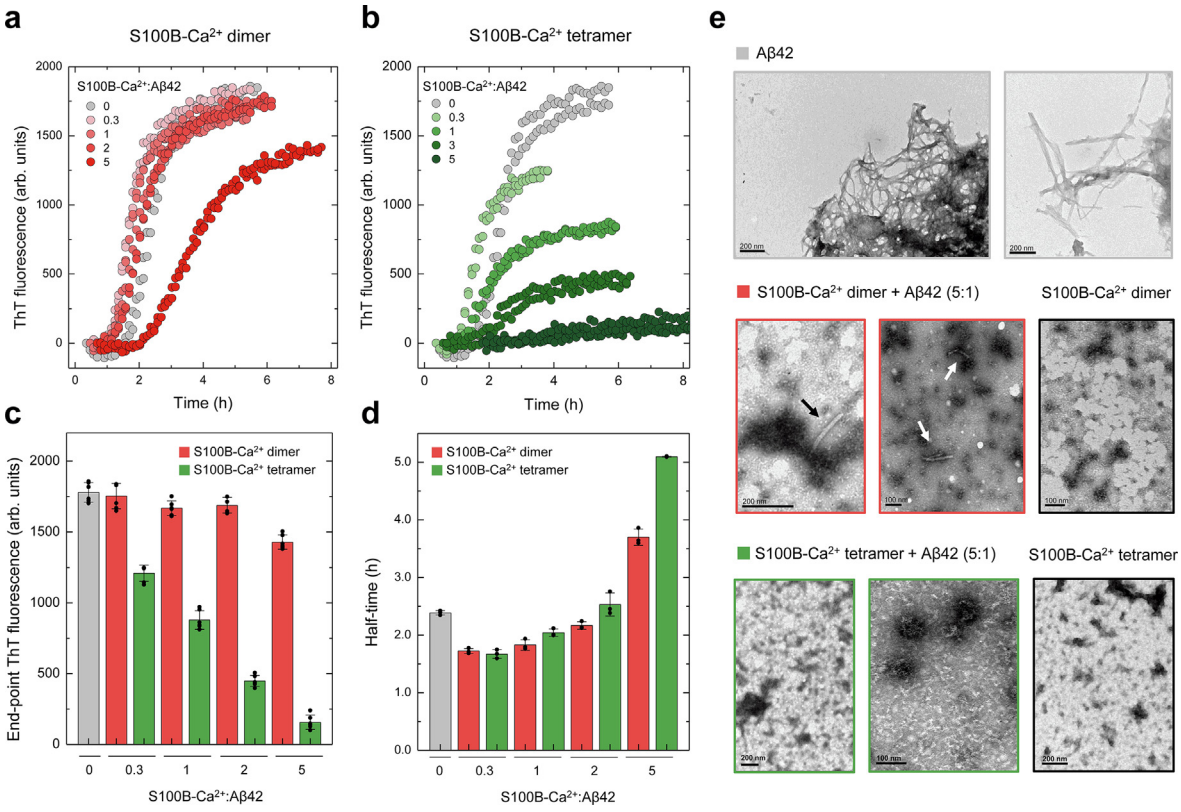

Figure 1. Effect of Ca^{2+}-bound S100B dimer and tetramer on the aggregation of monomeric Aβ42. (a, b) Kinetic traces of ThT-monitored aggregation of monomeric Aβ42 (3 μM) in the presence of 1.1 mM $CaCl_2$ and increasing concentrations (1 to 15 μM dimer equivalents) of **(a)** dimeric or **(b)** tetrameric S100B. Effects of dimeric (red) and tetrameric (green) S100B-Ca^{2+} on **(c)** the relative fibril mass inferred from the final ThT-intensity at the end point of kinetic traces (t > 10 h) and on **(d)** the aggregation half-times, in hours, on the different conditions tested, versus the Aβ42 (3 μM) control alone (gray). Error bars represent standard deviation of at least 3 experiments. See supplemental Figure 2 for fits of kinetic traces. **(e)** Representative transmission electron microscopy images of Aβ42 aggregation endpoints at a S100B-Ca^{2+}:Aβ42 molar ratio of 5 in the presence of dimeric (red contour) and tetrameric (green contour) S100B-Ca^{2+}, versus appropriate controls with 15 μM dimeric and tetrameric S100B-Ca^{2+} alone (black contour) and Aβ42 (grey contour). Black and white arrows pinpoint short sparse Aβ42 fibrils observed in the presence of dimeric S100B-Ca^{2+}. Scale-bars are indicated in each TEM image.

the aggregates formed at the endpoints of the Aβ42 aggregation reaction, in the absence and presence of Ca^{2+}-bound dimeric and tetrameric S100B (Figure 1(**e**)). For the Aβ42 control, as expected, we found large amounts of amyloid-like fibrils with a high degree of self-stacking. In the presence of the S100B-Ca^{2+} dimer, mostly amorphous aggregates are observed with only a few sparse shorter fibrils observed (Figure 1(**e**), **red contoured images**). Notably, in the presence of tetrameric S100B-Ca^{2+} we exclusively observed non-amyloid polymorphic aggregates (Figure 1(**e**), **green contoured images**) without any fibrillar or pre-fibrillar species. From TEM immuno-gold labelling experiments, we observed that Aβ42 labelling is exclusively associated to fibrils while S100B labelling is observed in amorphous aggregates (see Supplementary Figure 3). Indeed, the formation of S100B oligomers has been noted previously[12] and is further corroborated by TEM imaging of the S100B-Ca^{2+} dimer and tetramer in which oligomers are also observed but no fibrillar materials, as expected (Figure 1(**e**), **black contoured images**). Thereby, TEM bioimaging corroborates the kinetic assays findings, which indicate that tetrameric S100B-Ca^{2+} is more competent to suppress Aβ42 aggregation than the S100B-Ca^{2+} dimer.

Structural analysis uncovers a novel extended hydrophobic surface on tetrameric S100B

We then investigated which structural features of the S100B tetramer might account for its increased chaperone activity in respect to those of the S100B dimer. We previously established that in the Ca^{2+}-bound S100B dimer, Aβ42 binds to a cleft formed at the S100B dimer interface by a pair of contiguous helices IV, one from each S100B monomer, that comprise residues with high

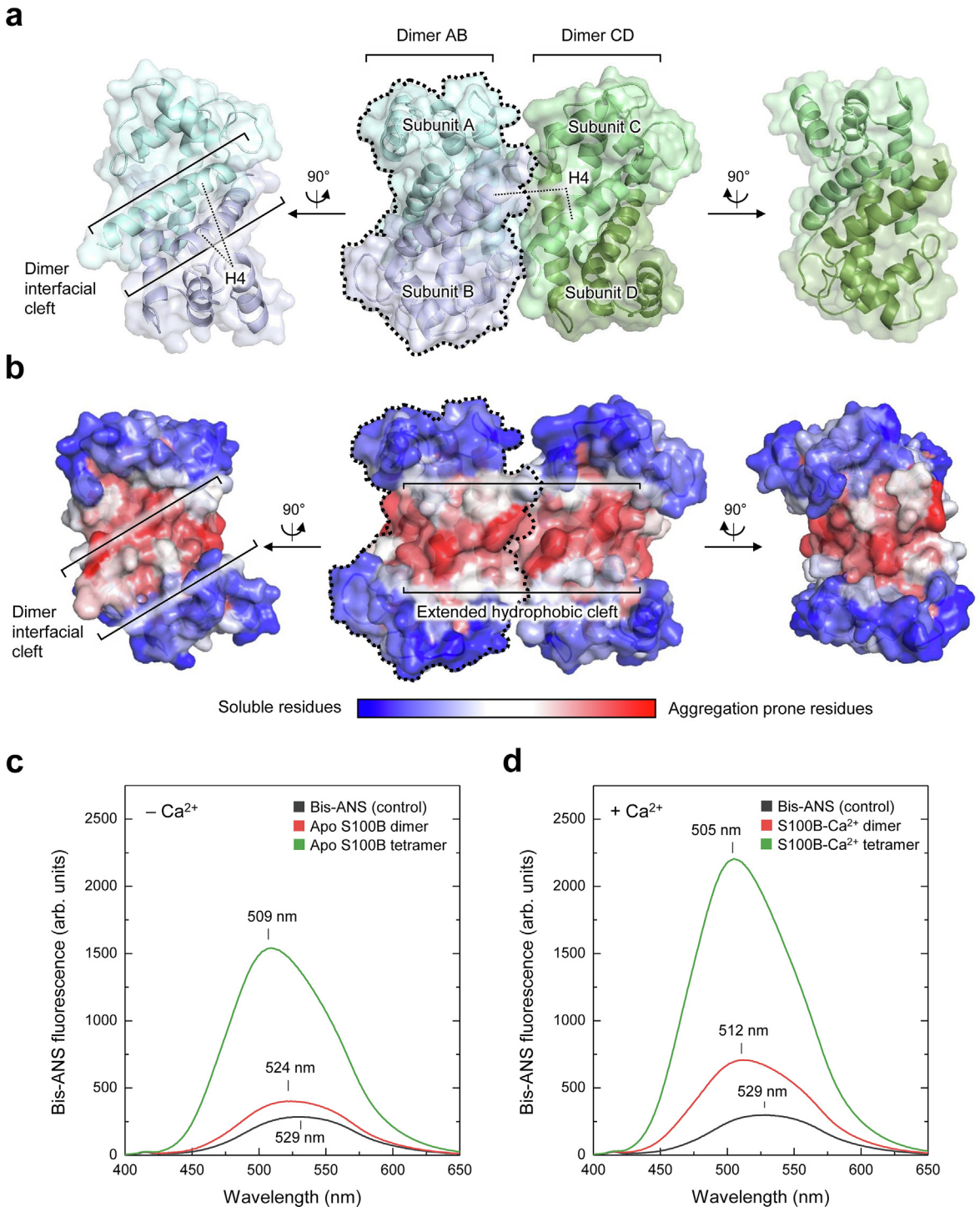

Figure 2. Aggrescan3D analysis of the S100B tetramer uncovers an extended cleft composed by aggregation-prone and hydrophobic residues, formed by the lateral assembling of two dimers. (a) Structural representation of the crystal structure of the S100B tetramer (PDB ID: 2H61) formed by stacking of two pairs of dimers, highlighting all of the four subunits (A to D) and the two previously known dimer interfacial clefts; **(b)** Aggrescan3D analysis of the same structure, depicted in the same orientation, highlighting the newly identified extended hydrophobic cleft formed by lateral juxtaposition of two dimers. Residues are color-coded according to their aggregation score. **(c, d)** Bis-ANS fluorescence emission spectra in the presence of dimeric or tetrameric S100B (15 μM dimer equivalents) in the absence **(c)** and in the presence **(d)** of Ca^{2+}. Maximum emission wavelengths, in nm, are indicated.

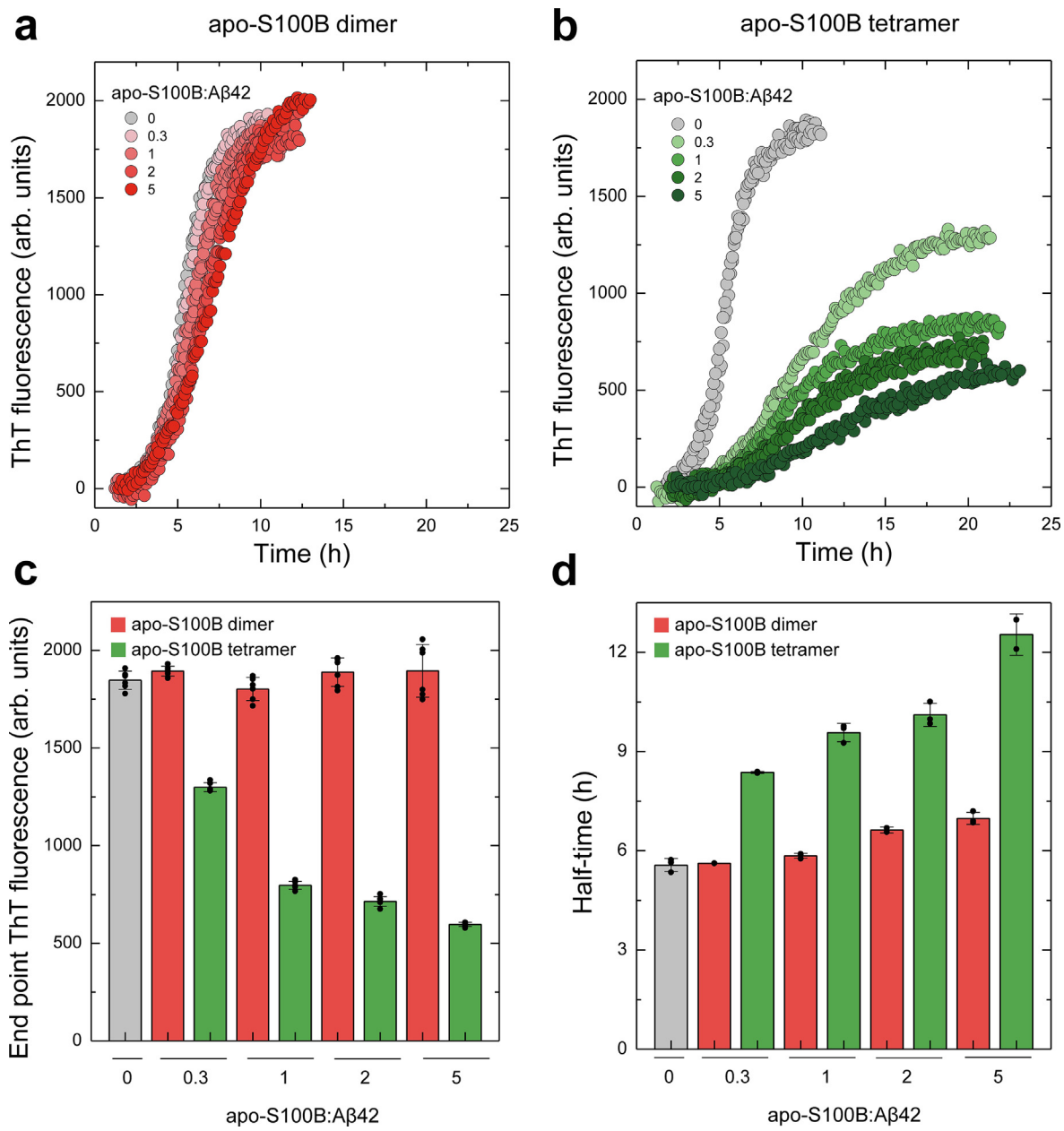

Figure 3. Effect of dimeric and tetrameric apo-S100B on the aggregation of monomeric Aβ42**. (a,b)** Kinetic traces of ThT-monitored aggregation of monomeric Aβ42 (3 μM) in the presence of 1.1 mM EDTA and increasing concentrations (1 to 15 μM dimer equivalents) of **(a)** dimeric or **(b)** tetrameric S100B. Effects of dimeric (red) and tetrameric (green) apo-S100B on **(c)** the relative fibril mass inferred from the final ThT-intensity at the end point of kinetic traces (t > 25 h) and on **(d)** the aggregation half-times, in hours, on the different conditions tested, versus the Aβ42 (3 μM) control alone (gray). Error bars represent standard deviation of at least 3 experiments. See supplemental Figure 2 for fits of kinetic traces.

aggregation propensity (Supplementary Figure 4 (**a**), (**b**)).[12,33] Such studies established that the regulatory interactions between S100B and the Aβ42 are mediated by transient heterotypic interactions formed between hydrophobic aggregation prone regions in the chaperone cleft and its amyloidogenic client.[12] Driven by this knowledge, we set to investigate if the increased chaperone efficiency of the S100B-Ca^{2+} tetramer might result from exposure of additional regions with high hydrophobic character and increased aggregation propensity. For this we set out to pinpoint such regions on the S100B tetramer crystallographic structure (Figure 2(**a**)), using the Aggrescan3D predictor.[34] This algorithm accurately predicts aggregation prone hot-spots in proteins based not only on primary sequence features, but also three-dimensional structure.[34] Remarkably, this analysis revealed that tetrameric

S100B comprises an additional extended aggregation-prone surface that is formed by the lateral juxtaposition of two helixes IV, each from one dimer interfacial cleft (Figure 2(**b**)). This region corresponds to the S100B C-terminus domain which, as also predicted by sequence-based algorithms,[35–36] comprises aggregation prone segments and several hydrophobic residues, notably Met79, Phe87 and Phe88 (Supplementary Figure 4 (**b**)). As the activity of anti-aggregation chaperones involves hydrophobic surfaces that mediate interactions with amyloidogenic clients[37–38], we postulated that this extended hydrophobic surface cleft in the S100B tetramer is a likely regulatory site amenable to interact with monomeric Aβ42.

To obtain further experimental validation for increased hydrophobic surface exposure in the S100B-Ca^{2+} tetramer, we resorted to the hydrophobicity sensitive fluorophore Bis-ANS.[39] We started by validating the assay analysing the

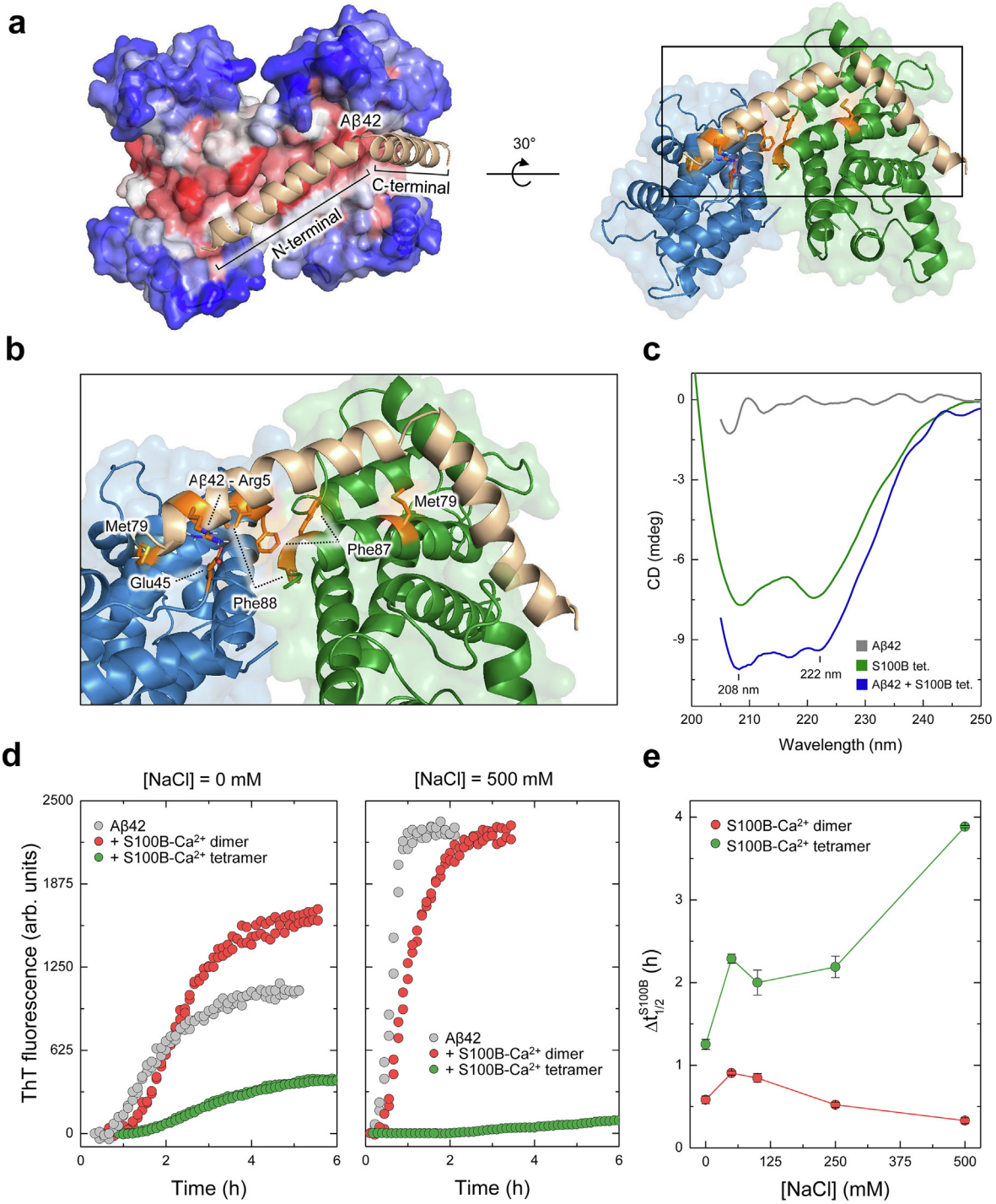

S100B dimer, which essentially does not bind Bis-ANS in the absence of Ca^{2+} (Figure 2(**c**)**, red trace**) in agreement with the fact that under these conditions the protein exposes no hydrophobic surfaces. However, Ca^{2+}-binding to the S100B dimer triggers a conformational change involving a movement of helix III that leads to exposure of an hydrophobic patch[40]; accordingly, we observe an increase in Bis-ANS fluorescence and a blue shift in the emission of dimeric S100B-Ca^{2+} (Figure 2(**d**)**, red trace**). The situation is however drastically different in the S100B tetramer: while a considerable enhancement on Bis-ANS fluorescence is also observed in the Ca^{2+}-bound form (Figure 2(**d**)**, green trace**), the fact is that a fluorescence enhancement it is also noticed in the apo, Ca^{2+}-free S100B tetramer (Figure 2(**c**)**, green trace**). We have demonstrated that Bis-ANS enhancement is due to the S100B tetramer and not to the minor high molecular weight species eluting as a shoulder by monitoring Bis-ANS enhancement in the eluted fractions and verifying that the minor species do not contribute to emitted fluorescence (Supplementary Figure 1(**e**)). Overall, these results indicate that, unlike the dimer, the S100B tetramer exposes a substantial hydrophobic surface in the apo-state, which is in perfect agreement with the extended hydrophobic cleft evidenced by the Aggrescan3D structural analysis.

The extended hydrophobic cleft in tetrameric S100B mediates Ca^{2+}-independent interactions with monomeric Aβ42

We next hypothesized that the Ca^{2+} independent extended hydrophobic cleft in tetrameric S100B might account for the enhanced anti-aggregation activity by providing an additional regulatory surface for interactions with Aβ42. To test this possibility, we investigated the effect of apo-S100B tetramer on the aggregation of Aβ42, as such experiment would allow to exclude interactions at the previously identified dimer interfacial cleft, whose exposure is dependent of Ca^{2+}-binding.[12] Indeed, we observed that, unlike the S100B dimer (Figure 3(**a**)), Ca^{2+}-free tetrameric S100B is a strikingly competent aggregation inhibitor of Aβ42 aggregation, even at sub stoichiometric molar ratios (Figure 3(**b**)**,** (**c**)**,** (**d**))**.** This finding supports the hypothesis that the S100B tetramer extended hydrophobic cleft constitutes an additional binding site for Aβ42 that accounts for enhanced anti-aggregation activity.

To examine this possibility from a computational structural biology perspective, we next performed docking analysis between the 100B tetramer and monomeric Aβ42 using HADDOCK.[41] Our preceding work revealed that the interaction of Aβ42 with the Ca^{2+} dependent binding clef at the S100B dimer interface is accompanied by a folding-upon-binding process that stabilizes Aβ42 in an helical configuration.[12] Indeed, in solution, unfolded Aβ is in equilibrium with the respective helical conformation.[42–43] Using this knowledge, we previously analysed the docking between Aβ42 and the Ca^{2+} dependent cleft on the S100B dimer employing an Aβ42 conformer on an α-helical conformation and with a kink,[17] resembling the NMR experimental structure.[44] To access if we could use Aβ42 in the same helical configuration to investigate its docking to the Ca^{2+} independent extended binding cleft in the S100B tetramer, far-UV CD spectroscopy experiments were performed to establish if the interaction Aβ42 with the S100B tetramer also results α-helical gain. For this we monitored the conformational changes occurring upon the addition of a 2-fold excess of freshly prepared monomeric Aβ42 to tetrameric S100B, in the absence of Ca^{2+} and in respect to adequate controls. Indeed, we observed an increase in ellipticity at 208 nm and 222 nm denoting a gain in α-helical structure which is compatible with gain of structure of monomeric Aβ42 upon its interaction with tetrameric S100B (Figure 4 (**c**)). Consequently, we posit that upon interaction with the S100B tetramer, Aβ42 monomers tend to adopt an α-helical conformation, thus validating the docking analysis using Aβ42 in a helical configuration.

Figure 4. Docking analysis of monomeric Aβ42 interaction with the extended hydrophobic surface on the S100B tetramer. (a) Haddock best docking pose cluster (score = –132.7 ± 7.1) depicting the interaction between monomeric helical Aβ42 (wheat coloured) and the S100B tetramer extended cleft (represented in the left panel as a surface with Aggrescan3D colour code and in the right panel as a cartoon with each composing dimers coloured in blue and green). **(b)** Zoom-in representation of the best docked structure highlighting hydrophobic and charged residues (orange-coloured) involved in interactions with Aβ42. **(c)** Far-UV CD spectrum of the apo-S100B tetramer incubated with Aβ42 at a molar ratio Aβ42:S100B = 2 (blue) versus appropriate controls of the two proteins alone at the same concentrations as in the mixture. tetrameric S100B (5 μM dimer equivalents, green) and monomeric Aβ42 (10 μM, grey). **(d)** Kinetic traces of ThT-monitored aggregation of monomeric Aβ42 (4 μM) in the presence of 1.1 mM $CaCl_2$ and 20 μM (dimer equivalents) of dimeric (red) and tetrameric (green) S100B-Ca^{2+} at low (left, [NaCl] = 0 mM) and high (right, [NaCl] = 500 mM) ionic strength. **(e)** Effect of ionic strength on the aggregation half-time of monomeric Aβ42 (4 μM) in the presence of 20 μM (dimer equivalents) of dimeric (red) and tetrameric (green) S100B-Ca^{2+} ($\Delta t_{1/2}^{S100B}$). Error bars represent standard deviation of at least 3 experiments. See supplemental Figure 2 for fits of kinetic traces.

Notably, the best docking pose cluster (HADDOCK score −132.7 ± 7.1) perfectly matches the interaction of Aβ42 with the extended hydrophobic cleft on tetrameric S100B (Figure 4 (**a**)**, left**). In addition to contacts between Aβ42 C-terminal end the same residues from the helices IV that are implicated in the previously identified S100B dimer interfacial cleft and that have thus been already experimentally validated,[12] the depicted docking solution shows that the Aβ42 N-terminal segment is further stabilized by hydrophobic interactions established with residues at the S100B tetramer extended surface (Figure 4(**a**)**, right**). Indeed, side chains from Met79, Phe87 and Phe88 residues from two distinct S100B dimers are correctly oriented to interact with the Aβ42 N-terminal region (Figure 4(**b**)). Furthermore, structural analysis elicits a possible electrostatic interaction between Aβ42-Arg5 and S100B-Glu45. To experimentally access the significance of hydrophobic contacts for Aβ42:S100B tetramer interactions, we tested how increasing ionic strength, generated by varying NaCl concentration, would affect the inhibition of Aβ42 aggregation by S100B (Figure 4(**d**)**,** Supplementary Figure 5). In addition to interfere with the formation of ionic interactions, high salt will favour nonpolar interactions through desolvation effects.[45] Given that ionic strength influences Aβ42 fibrillation,[46] we opted to evaluate inhibitory effects of S100B as the increase on aggregation half-time caused by the presence of the chaperone ($\Delta t_{1/2}^{S100B}$) (Figure 4(**e**)). Remarkably, when we compare the chaperone activities of dimeric and tetrameric S100B-Ca^{2+} over a wide range of NaCl concentrations, results show that the activity of tetrameric S100B is strongly augmented by increasing ionic strength, corroborating the predominant involvement of non-polar interactions. This trend diverges from that observed for the S100B dimer, whose anti-aggregation activity does not increase with at higher ionic strength (Figure 4(**d**)**,** (**e**)).

Overall, computational and experimental findings provide evidence for an interaction between monomeric Aβ42 and tetrameric S100B, whose increased anti-aggregation activity is likely the result of multivalent Ca^{2+}-independent interactions that involve the newly identified extended hydrophobic surface on tetrameric S100B.

Tau aggregation is poorly inhibited by tetrameric S100B

Lastly, we tested if the oligomerization state of the S100B chaperone could modulate its client preference or increase its effect on tau aggregation. We recently uncovered that dimeric S100B-Ca^{2+} strongly counteracts tau aggregation by interacting with tau microtubule binding regions (MTBR) in a Ca^{2+}-dependent mode.[13] Structural NMR data revealed that, as for Aβ42, interaction with tau MTBR encompass contacts mostly with the cleft formed at the S100B dimer interface involving helices IV, but also with the contiguous orthogonal helix III.[13] Again, we employed ThT-monitored aggregation kinetic assays to access the anti-aggregation activity of dimeric and tetrameric S100B, in the apo and Ca^{2+}-bound state, over the K18 tau fragment which includes MTBR segments and recapitulates the main properties of human full-length tau aggregation.[47] While the S100B-Ca^{2+} dimer strongly inhibits tau K18 aggregation even at sub stoichiometric levels, as previously noted (Figure 5(**a**)**,** (**c**)**,** (**d**)), tetrameric S100B-Ca^{2} is prominently a less competent chaperone (Figure 5(**b**)**,** (**c**)**,** (**d**)). Indeed, only a mild delay on aggregation is observed at a S100B:K18 molar ratio of 0.5, with no reduction of K18 fibrillar mass, while negligible effects were observed at lower molar ratios.

We conjecture that the lower chaperone activity of the S100B tetramer in respect to tau aggregation likely results from the fact that tetramerization impairs the dynamics of the tau interacting regions in the S100B dimer, that involve not only the interfacial cleft formed by helices IV but also with contiguous helix III, which is not implicated in interactions with Aβ42. Also, the fact that the apo-S100B tetramer did not affect tau K18 aggregation (**Supplementary Figure 6**) also rules out an interaction with the extended hydrophobic surface on the tetramer. Therefore, we posit that the S100B tetramer has evolved a regulatory surface that is amenable to establish preferential interactions with the Aβ42 client but not with tau, evidencing a functional plasticity and fine tuning of activity, that may be critical to handle different proteotoxic insults during distinct stages of Alzheimer's progression.

Conclusions

Multimerization is known to be relevant for several molecular chaperones, including small heat-shock proteins (HSPs),[30] the Bri2 BRICHOS domain[31] and Trigger Factor[29], which in some cases modulates the microscopic mechanisms through which chaperones suppress amyloid formation.[48–49] Indeed, disulfide cross-linked S100B multimers formed by Cu^{2+}-induced Cys84 oxidation were reported to have improved suppression activity of Aβ42 aggregation. Nevertheless, the three-dimensional arrangement of S100B -S—S- covalently-bound multimers differs from that of the non-covalent oligomers.[15] Motivated by this set of evidence, we here tested the hypothesis that the chaperone activity might be augmented in the S100B tetramer, which is found in the human brain. Indeed, we uncovered that this is the case and that this results from a novel extended hydrophobic surface that mediates Ca^{2+}-independent interactions with monomeric Aβ42. This novel regulatory surface spawned by S100B tetramerization effectively expands the catalytic ability of the chaperone as it

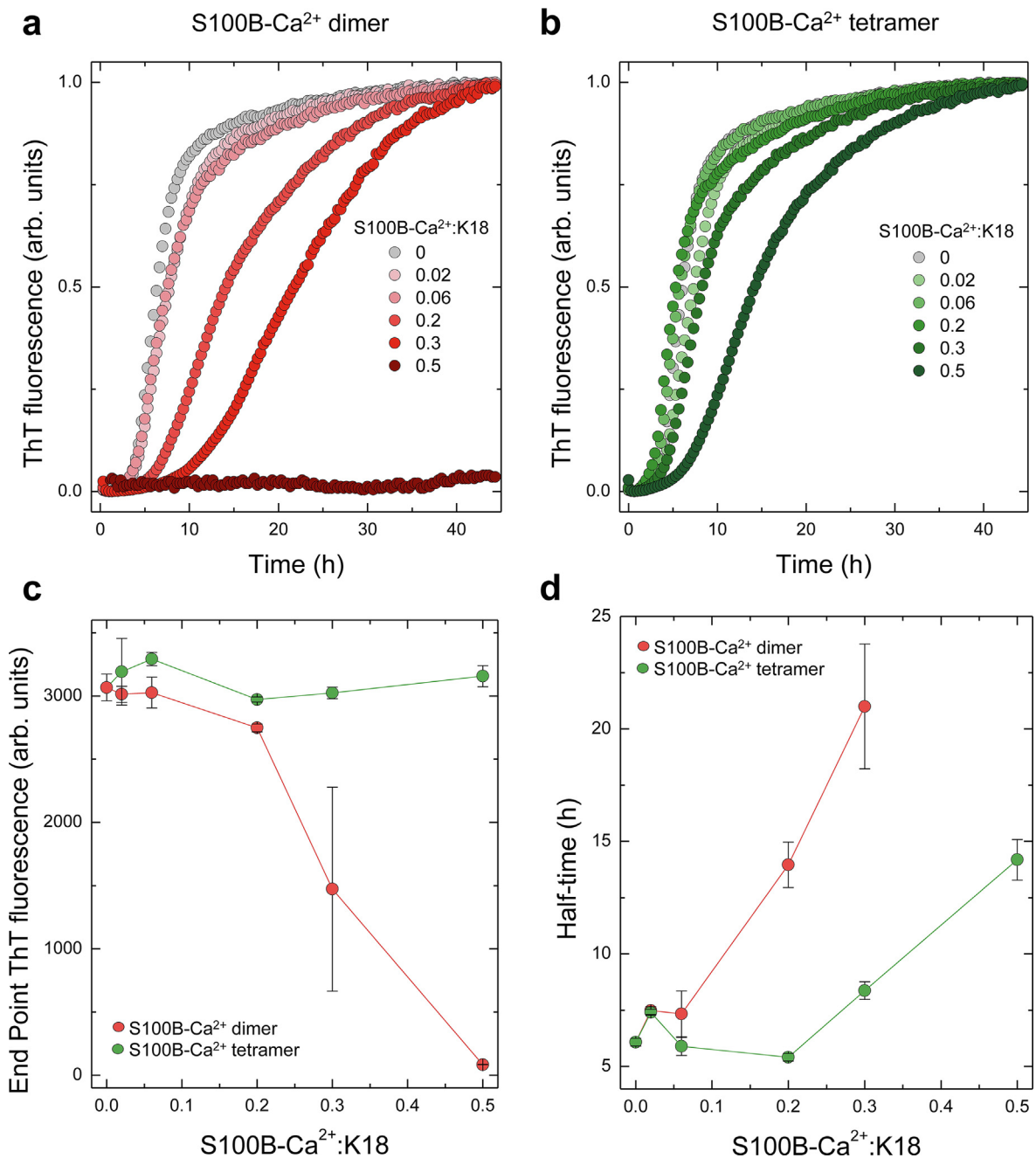

Figure 5. Effect of S100B dimer and tetramer over K18 tau fragment aggregation. (a, b) Normalized kinetic traces of ThT-monitored aggregation of K18 (10 μM) in the presence of 1.1 mM $CaCl_2$ and increasing concentrations (0.2 to 5 μM dimer equivalents) of **(a)** dimeric or **(b)** tetrameric S100B-Ca^{2+}. **(c)** Relative Tau-K18 fibril mass inferred from the final ThT-intensity at the end point of kinetic traces (t > 45 h) and **(d)** aggregation half-times, in hours, of the different conditions tested. Error bars represent standard deviation of at least 3 experiments. See supplemental Figure 2 for fits of kinetic traces.

mediates interactions with monomeric Aβ42 which do not require conformational changes induced by Ca^{2+}-binding. In terms of Aβ42 aggregation steps affected by tetrameric S100B, interactions with monomeric Aβ42 indicate an effect on primary nucleation and subsequent steps involving monomers, while the preferential colocalization with Aβ42 fibrils detected in TEM immunogold labeling experiments suggests interactions with fibril surfaces and possibly also with oligomers, suggesting an effect on secondary nucleation processes. Therefore, tetramerization effectively expands the catalytic repertoire of the S100B chaperone, as this regulatory surface operates concertedly with the

previously known Aβ42 binding cleft at the dimer interface. The multivalence afforded by tetramerization affords not only enhanced activity, as lower molar ratio of client:chaperone is sufficient to counteract Aβ42 aggregation independently of Ca^{2+}-binding, but also substrate specificity, as interactions with the tau substrate at this secondary site are deterred versus those with Aβ42. We hypothesize that this functional fine-tuning of the S100B chaperone associated with tetramerization will be important in the response to different types and intensities of proteotoxic insults during Alzheimer's disease progression, an aspect that will be clarified by future research in our laboratories.

Materials and Methods

Materials and proteins

All reagents were of the highest grade commercially available. A chelex resin (Bio-Rad) was used to remove contaminant trace metals from all buffers. Recombinant Aβ42 was expressed in *Escherichia coli* and purified as described.[50] To obtain the monomeric form, about 2 mg of Aβ42 was dissolved in 7 M guanidine hydrochloride (Sigma) and eluted in a Superdex S75 (GE Healthcare) with 50 mM HEPES (4-(2-hydroxyethyl)-1-piperazineethanesulfonic acid, NZYtech) pH7.4. Monomeric Aβ42 concentration was estimated by UV spectroscopy (SPECTROstar Nano BMG LabTech) at 280 nm using the theoretical extinction coefficient value of $\varepsilon_{280\ nm} = 1424\ M^{-1}$-$cm_{-1}$. K18 tau fragment was recombinantly expressed in *E. coli* and purified as described.[13] Low-binding tubes (Axygen Scientific, Corning) were used in all manipulations of Aβ42 of K18. Human S100B was also expressed in *E. coli* and purified to homogeneity as described.[28,32] Analysis and isolation of dimeric/tetrameric S100B obtained after purification was performed by size exclusion chromatography at room temperature on a Superdex 75 Tricorn high performance column (GE Healthcare, bed volume = 24 mL) eluted at 1 mL/min with 50 mM Tris-HCl (tris(hydroxymethyl)amino methane, NZYtech) pH7.4. During S100B tetramer isolation, the fractions corresponding to the initial elution shoulder were discarded, to avoid possible contamination with higher-order species. Dimer and tetramer S100B concentration were estimated as homodimer equivalents by UV spectroscopy at 280 nm using the theoretical extinction coefficient value of $\varepsilon_{280\ nm} = 2980\ M^{-1}cm^{-1}$.

Electrophoretic assays

SDS-PAGE analysis S100B multimers under reducing/nonreducing conditions was carried out using an 8% acrylamide (NZYtech) gel. Samples were incubated with 150 mM Tris-HCl pH6.8 loading buffer containing 6% (m/v) SDS with or without 10% (v/v) β-mercaptoethanol (Sigma) for 10 minutes at 100 °C. After incubation, samples were loaded into the gel (3 μg/well) and subsequently separated for about 1.5 h at 150 V. Low Molecular Weight II (NZYtech) Protein Markers were used as standards. Proteins were detected by gel treatment with BlueSafe reagent (NZYTech). For Native Blue PAGE, dimeric and tetrameric S100B samples were mixed with 50 mM Tris + 50 mM MOPS (3-(morpholin-4-yl)propane-1-sulfonic acid, Applichem) pH7.7 native loading buffer containing 0.02% (m/v) Coomassie brilliant blue G250 (Sigma). 3 μg of protein were loaded into a pre-casted NativePAGE 4 to 16% Bis-Tris gel (Invitrogen). Electrophoretic run was performed during 40 minutes at 200 V using similar cathode and anode buffers. Proteins were detected by Coomassie staining.

CD spectroscopy

Circular dichroism (CD) measurements were performed on a Jasco J-1500 spectropolarimeter equipped with a Peltier-controlled thermostated cell support at 25 °C. Samples were prepared by diluting S100B tetramer to a final concentration of 5 μM (dimer equivalents) in 50 mM Tris-HCl pH 7.4 with and without a 2-*fold* excess of monomeric Aβ42 following a 1 h incubation at room temperature. Far UV-CD spectra were recorded between 195/205 nm and 260 nm using a 1 mm pathlength quartz cuvette (Hellma Analytics) and a minimum of 12 scans of average accumulation. Before smoothened, buffer baselines were subtracted from each spectrum.

Fluorescence spectroscopy

Bis-ANS (4,4′-Dianilino-1,1′-binaphthyl-5,5′-disulfonic acid) fluorescence measurements were performed on a Jasco FP8200 spectrofluorometer at 25 °C. Dimeric and tetrameric S100B (both at 15 μM dimer equivalents) were incubated with a 2-*fold* excess of Bis-ANS (Sigma) in 50 mM HEPES pH7.4 for 2 h at 25 °C. For the experiments in the presence of calcium, 2 μL of a 5 mM $CaCl_2$ stock solution were added to each sample (with 60 μL of total volume) and incubated for additional 5 minutes at 25 °C. Bis-ANS emission spectra were recorded between 375 nm and 650 nm using an excitation wavelength of 365 nm, 5 nm of excitation/emission bandwidths and 4 scans of average accumulation.

Aggregation kinetics

Aβ42 and K18 aggregation kinetics were performed by recording Thioflavin-T (ThT) fluorescence intensity as a function of time in a plate reader (FLUOstar Optima, BMG Labtech) with a 440 nm excitation filter and a 480 nm emission filter. The fluorescence was measured using bottom optics in half-area 96-well

polyethylene glycol-coated black polystyrene plates with a clear bottom (Corning, 3881). The microplates were sealed with foil to avoid evaporation. Monomeric Aβ42 was diluted to a final concentration of 3 μM in 50 mM HEPES pH7.4 with 1.1 mM $CaCl_2$ (Sigma) or 1.1 mM EDTA (ethylenedinitrilotetraacetic acid, Sigma) and the indicated concentrations of dimeric and tetrameric S100B (both expressed in terms of dimer equivalents). 6 μM of ThT (Sigma) was added to each condition. For kinetic assays at varying ionic strengths, Aβ42 monomers were diluted to a final concentration of 4 μM with or without 20 μM of S100B dimer/tetramer in 50 mM HEPES pH7.4 with 1.1 mM $CaCl_2$, 8 μM ThT and the specified concentrations of NaCl (sodium chloride, NZYTech). The K18 tau fragment was diluted to a concentration of 10 μM in 50 mM Tris-HCl pH7.4 with 1.1 mM $CaCl_2$ or 0.5 mM EDTA, 1 mM DTT (dithiothreitol, Applichem), 50 mM NaCl, 75 μM ThT, 5 μM heparin sulphate (Sigma) to induce aggregation, and the indicated concentrations of dimeric and tetrameric S100B. All assays were performed at 37 °C, under quiescent conditions and fluorescence measurements taken every 400 seconds. Aggregation kinetic data and reaction half times were analysed using AmyloFit.[51] The error bars represent standard deviation between different technical replicates (n = 3).

Transmission electron microscopy

For the analysis of structure and morphology of samples at the end-point of the aggregation reactions, 5 μL sample aliquots were adsorbed into carbon-coated collodion film supported on 300-mesh copper grids (Electron Microscopy Sciences) and negatively stained twice with 1% (m/v) uranyl acetate (Electron Microscopy Sciences). For immunogold labelling, 5 μL-sample aliquots were adsorbed to carbon-coated collodion film supported on 300-mesh nickel grids (Electron Microscopy Sciences). Grids were then blocked with 1% bovine serum albumin (BSA) for 10 min, followed by incubation with anti-S100B monoclonal antibody from rabbit (1:50, Cat. ab52642, Abcam, Cambridge, UK), or BAM-10 anti-Aβ peptide monoclonal antibody from mouse (1:50, Cat. MA1-91209, Invitrogen, USA), for 30 min. Following washing with PBS, grids were then incubated with either anti-rabbit or anti-mouse secondary antibodies conjugated to 10- or 6-nm colloidal gold, respectively, for 20 min. Finally, samples were negatively stained twice with 1% (m/v) uranyl acetate. As control, grids with sample adsorbed and blocked as described, were incubated with secondary antibodies only, and then negatively stained. Grids were visualized with a JEOL JEM-1400 transmission electron microscope equipped with an Orious Sc1000 digital camera, and exhaustively observed.

Structural analysis and docking

All structures were visualized and manipulated in PyMOL (Version 2.4.1, Schrödinger). S100B octamer crystallographic structure was obtained in Protein Data Bank (PDB ID: 2H61) in Dec/2021 and stripped of water molecules. The S100B tetramer was built from this structure by deleting dimers EF and GH.[26] Prediction of aggregation prone hots-spots in S100B tetramer structure was performed in Aggrescan3D (Version 2.0)[34] using non-dynamic mode a 10 Å distance of aggregation analysis. Calcium and zinc bound S100B dimer crystallographic structure[52] was obtained in Protein Data Bank (PDB ID: 3D0Y) in Mar/2022 and submitted to an identical workflow. Docking calculations were done using the Haddock web server 2.4[41,53] with standard parameters. The Aβ42 helical model used as input has been previously described[17] and all 42 residues of the Aβ42 peptide were assigned as active. For tetrameric S100B, residues from helix IV (Gln72 to His91) corresponding to the conventional and extended hydrophobic clefts identified in Aggrescan3D, were assigned as active, with passive residues assigned automatically. The best cluster of docking poses (with the lowest Haddock score) was considered for analysis, as this solution correctly predicted the NMR validated binding mode of Aβ42 C-terminus and S100B dimer interfacial cleft.

Author Contributions

C.M.G. conceived, designed, and supervised the study, analysed data, and wrote the manuscript with A.J.F. Experiments were designed, conducted, and analysed by A.J.F., G.G.M., J.S. and I.C. All authors revised and approved the manuscript.

Notes

The authors declare no competing financial interests.

Acknowledgement

This work was funded by the LabCollector Scientific Award 2021 (Agilebio, France) (to C.M.G) and by Fundação para a Ciência e Tecnologia (Portugal) through research PTDC/MED-PAT/0959/2021 (to I.C.) and PhD fellowships BD/06393/2021 (to A.J.F.), DFA/BD/6443/2020 (to G.G.M.), fellowship BID/FCT_Pro j2020/i3S/23110712/2021 (to J.S.) and center grants UID/MULTI/04046/2020 (to BioISI) and Norte-01-0145-FEDER-000008 (to IBMC/I3S). We thank the support of the i3S Histology and Electron Microscopy Scientific platform.

Appendix A. Supplementary Data

Supplementary data to this article can be found online at https://doi.org/10.1016/j.jmb.2022.167791.

Received 5 June 2022;
Accepted 9 August 2022;
Available online 12 August 2022

Keywords:
Amyloid-β;
tau;
S100 protein;
molecular chaperone;
protein aggregation

References

1. Masters, C.L., Bateman, R., Blennow, K., Rowe, C.C., Sperling, R.A., Cummings, J.L., (2015). Alzheimer's disease. *Nat. Rev. Dis. Primers.* **1**, 15056.
2. Cuello, A.C., (2017). Early and Late CNS Inflammation in Alzheimer's Disease: Two Extremes of a Continuum? *Trends Pharmacol. Sci.* **38**, 956–966.
3. Heneka, M.T., Golenbock, D.T., Latz, E., (2015). Innate immunity in Alzheimer's disease. *Nat. Immunol.* **16**, 229–236.
4. Marshak, D.R., Pesce, S.A., Stanley, L.C., Griffin, W.S.T., (1992). Increased S100β neurotrophic activity in Alzheimer's disease temporal lobe. *Neurobiol. Aging* **13**, 1–7.
5. Cristovao, J.S., Gomes, C.M., (2019). S100 Proteins in Alzheimer's Disease. *Front Neurosci.* **13**, 463.
6. Donato, R., Sorci, G., Riuzzi, F., Arcuri, C., Bianchi, R., Brozzi, F., (2009). S100B's double life: Intracellular regulator and extracellular signal. Biochimica et Biophysica Acta (BBA) - Molecular. *Cell Res.* **1793**, 1008–1022.
7. Mori, T., Koyama, N., Arendash, G.W., Horikoshi-Sakuraba, Y., Tan, J., Town, T., (2010). Overexpression of human S100B exacerbates cerebral amyloidosis and gliosis in the Tg2576 mouse model of Alzheimer's disease. *Glia.* **58**, 300–314.
8. Austermann, J., Spiekermann, C., Roth, J., (2018). S100 proteins in rheumatic diseases. *Nat. Rev. Rheumatol.* **14**, 528–541.
9. Sorci, G., Bianchi, R., Riuzzi, F., Tubaro, C., Arcuri, C., Giambanco, I., (2010). S100B Protein, A Damage-Associated Molecular Pattern Protein in the Brain and Heart, and Beyond. *Cardiovasc. Psychiatry Neurol.* **2010**
10. Rouhiainen, A., Kuja-Panula, J., Tumova, S., Rauvala, H., (2013). RAGE-mediated cell signaling. *Methods Mol. Biol. (Clifton, NJ).* **963**, 239–263.
11. Baudier, J., Deloulme, J.C., Shaw, G.S., (2020). The Zn2+ and Ca2+-binding S100B and S100A1 proteins: beyond the myths. *Biol. Rev.* **95**, 738–758.
12. Cristóvão Joana, S., Morris Vanessa, K., Cardoso, I., Leal Sónia, S., Martínez, J., Botelho Hugo, M., (2018). The neuronal S100B protein is a calcium-tuned suppressor of amyloid-β aggregation. *Sci. Adv.* **4**, eaaq1702.
13. Moreira, G.G., Cantrelle, F.-X., Quezada, A., Carvalho, F. S., Cristóvão, J.S., Sengupta, U., (2021). Dynamic interactions and Ca2+-binding modulate the holdase-type chaperone activity of S100B preventing tau aggregation and seeding. *Nat. Commun.* **12**, 6292.
14. Cristovao, J.S., Figueira, A.J., Carapeto, A.P., Rodrigues, M.S., Cardoso, I., Gomes, C.M., (2020). The S100B Alarmin Is a Dual-Function Chaperone Suppressing Amyloid-beta Oligomerization through Combined Zinc Chelation and Inhibition of Protein Aggregation. *ACS Chem. Neurosci.* **11**, 2753–2760.
15. Cristóvão, J.S., Moreira, G.G., Rodrigues, F.E.P., Carapeto, A.P., Rodrigues, M.S., Cardoso, I., (2021). Cu (2+)-binding to S100B triggers polymerization of disulfide cross-linked tetramers with enhanced chaperone activity against amyloid-β aggregation. *Chem. Commun. (Camb.)* **57**, 379–382.
16. Hagmeyer, S., Cristóvão, J.S., Mulvihill, J.J., Boeckers, T. M., Gomes, C.M., Grabrucker, A.M., (2018). Zinc binding to S100B affords regulation of trace metal homeostasis and excitotoxicity in the brain. *Front. Mol. Neurosci.* **10**
17. Rodrigues, F.E.P., Figueira, A.J., Gomes, C.M., Machuqueiro, M., (2021). Computational Analysis of the Interactions between the S100B Extracellular Chaperone and Its Amyloid β Peptide Client. *Int. J. Mol. Sci.* **22**
18. Gilston, B.A., Skaar, E.P., Chazin, W.J., (2016). Binding of transition metals to S100 proteins. *Sci. China Life Sci.* **59**, 792–801.
19. Carvalho, S.B., Cardoso, I., Botelho, H.M., Yanamandra, K., Fritz, G., Gomes, C.M., (2014). Chapter 18 - Structural Heterogeneity and Bioimaging of S100 Amyloid Assemblies. In: Uversky, V.N., Lyubchenko, Y.L. (Eds.), *Bio-nanoimaging*. Academic Press, Boston, pp. 197–212.
20. Donato, R., (2001). S100: a multigenic family of calcium-modulated proteins of the EF-hand type with intracellular and extracellular functional roles. *Int. J. Biochem. Cell Biol.* **33**, 637–668.
21. Fritz, G., Botelho, H.M., Morozova-Roche, L.A., Gomes, C. M., (2010). Natural and amyloid self-assembly of S100 proteins: structural basis of functional diversity. *FEBS J.* **277**, 4578–4590.
22. Heizmann, C.W., Fritz, G., Schafer, B., (2002). S100 proteins: structure, functions and pathology. *Front. Biosci.* **7**, 1356–1368.
23. Xie, J., Burz, D.S., He, W., Bronstein, I.B., Lednev, I., Shekhtman, A., (2007). Hexameric Calgranulin C (S100A12) Binds to the Receptor for Advanced Glycated End Products (RAGE) Using Symmetric Hydrophobic Target-binding Patches*. *J. Biol. Chem.* **282**, 4218–4231.
24. Korndörfer, I.P., Brueckner, F., Skerra, A., (2007). The Crystal Structure of the Human (S100A8/S100A9)2 Heterotetramer, Calprotectin, Illustrates how Conformational Changes of Interacting α-Helices Can Determine Specific Association of Two EF-hand Proteins. *J. Mol. Biol.* **370**, 887–898.
25. Kiryushko, D., Novitskaya, V., Soroka, V., Klingelhofer, J., Lukanidin, E., Berezin, V., (2006). Molecular Mechanisms of Ca2+ Signaling in Neurons Induced by the S100A4 Protein. *Mol. Cell. Biol.* **26**, 3625–3638.
26. Ostendorp, T., Leclerc, E., Galichet, A., Koch, M., Demling, N., Weigle, B., (2007). Structural and functional insights into RAGE activation by multimeric S100B. *EMBO J.* **26**, 3868–3878.

27. Thulin, E., Kesvatera, T., Linse, S., (2011). Molecular determinants of S100B oligomer formation. *PLoS ONE* **6**, e14768.
28. Ostendorp, T., Heizmann, C.W., Kroneck, P.M.H., Fritz, G., (2005). Purification, crystallization and preliminary X-ray diffraction studies on human Ca2+-binding protein S100B. *Acta Crystall. Sect F Struct. Biol. Cryst. Commun.* **61**, 673–675.
29. Saio, T., Kawagoe, S., Ishimori, K., Kalodimos, C.G., (2018). Oligomerization of a molecular chaperone modulates its activity. *eLife* **7**, e35731.
30. Haslbeck, M., Vierling, E., (2015). A first line of stress defense: small heat shock proteins and their function in protein homeostasis. *J Mol Biol.* **427**, 1537–1548.
31. Chen, G., Abelein, A., Nilsson, H.E., Leppert, A., Andrade-Talavera, Y., Tambaro, S., (2017). Bri2 BRICHOS client specificity and chaperone activity are governed by assembly state. *Nat. Commun.* **8**, 2081.
32. Botelho, H.M., Fritz, G., Gomes, C.M., (2012). Analysis of S100 oligomers and amyloids. *Methods Mol. Biol. (Clifton, NJ).* **849**, 373–386.
33. Carvalho, S.B., Botelho, H.M., Leal, S.S., Cardoso, I., Fritz, G., Gomes, C.M., (2013). Intrinsically disordered and aggregation prone regions underlie β-aggregation in S100 proteins. *PloS One* **8**, e76629-e.
34. Kuriata, A., Iglesias, V., Pujols, J., Kurcinski, M., Kmiecik, S., Ventura, S., (2019). Aggrescan3D (A3D) 2.0: prediction and engineering of protein solubility. *Nucleic Acids Res.* **47**, W300–W307.
35. Cristóvão, J.S., Romão, M.A., Gallardo, R., Schymkowitz, J., Rousseau, F., Gomes, C.M., (2021). Targeting S100B with Peptides Encoding Intrinsic Aggregation-Prone Sequence Segments. *Molecules* **26**
36. Fernandez-Escamilla, A.M., Rousseau, F., Schymkowitz, J., Serrano, L., (2004). Prediction of sequence-dependent and mutational effects on the aggregation of peptides and proteins. *Nat. Biotechnol.* **22**, 1302–1306.
37. Kim, Y.E., Hipp, M.S., Bracher, A., Hayer-Hartl, M., Hartl, F.U., (2013). Molecular chaperone functions in protein folding and proteostasis. *Annu. Rev. Biochem.* **82**, 323–355.
38. Koldewey, P., Stull, F., Horowitz, S., Martin, R., Bardwell, J.C.A., (2016). Forces Driving Chaperone Action. *Cell* **166**, 369–379.
39. Younan, N.D., Viles, J.H., (2015). A Comparison of Three Fluorophores for the Detection of Amyloid Fibers and Prefibrillar Oligomeric Assemblies. ThT (Thioflavin T); ANS (1-Anilinonaphthalene-8-sulfonic Acid); and bisANS (4,4'-Dianilino-1,1'-binaphthyl-5,5'-disulfonic Acid). *Biochemistry* **54**, 4297–4306.
40. Charpentier, T.H., Wilder, P.T., Liriano, M.A., Varney, K. M., Zhong, S., Coop, A., (2009). Small molecules bound to unique sites in the target protein binding cleft of calcium-bound S100B as characterized by nuclear magnetic resonance and X-ray crystallography. *Biochemistry* **48**, 6202–6212.
41. Honorato, R.V., Koukos, P.I., Jiménez-García, B., Tsaregorodtsev, A., Verlato, M., Giachetti, A., (2021). Structural Biology in the Clouds. *WeNMR-EOSC Ecosyst.* **8**
42. Wei, G., Shea, J.-E., (2006). Effects of Solvent on the Structure of the Alzheimer Amyloid-β(25–35) Peptide. *Biophys. J.* **91**, 1638–1647.
43. D'Ursi, A.M., Armenante, M.R., Guerrini, R., Salvadori, S., Sorrentino, G., Picone, D., (2004). Solution structure of amyloid beta-peptide (25–35) in different media. *J. Med. Chem.* **47**, 4231–4238.
44. Tomaselli, S., Esposito, V., Vangone, P., van Nuland, N.A. J., Bonvin, A.M.J.J., Guerrini, R., (2006). The α-to-β Conformational Transition of Alzheimer's Aβ-(1–42) Peptide in Aqueous Media is Reversible: A Step by Step Conformational Analysis Suggests the Location of β Conformation Seeding. *ChemBioChem* **7**, 257–267.
45. Bogunia, M., Makowski, M., (2020). Influence of Ionic Strength on Hydrophobic Interactions in Water: Dependence on Solute Size and Shape. *J. Phys. Chem. B* **124**, 10326–10336.
46. Meisl, G., Yang, X., Dobson, C.M., Linse, S., Knowles, T.P. J., (2017). Modulation of electrostatic interactions to reveal a reaction network unifying the aggregation behaviour of the Aβ42 peptide and its variants. *Chem. Sci.* **8**, 4352–4362.
47. Shammas, S.L., Garcia, G.A., Kumar, S., Kjaergaard, M., Horrocks, M.H., Shivji, N., (2015). A mechanistic model of tau amyloid aggregation based on direct observation of oligomers. *Nat. Commun.* **6**, 7025.
48. Arosio, P., Michaels, T.C., Linse, S., Mansson, C., Emanuelsson, C., Presto, J., (2016). Kinetic analysis reveals the diversity of microscopic mechanisms through which molecular chaperones suppress amyloid formation. *Nat. Commun.* **7**, 10948.
49. Chen, G., Andrade-Talavera, Y., Tambaro, S., Leppert, A., Nilsson, H.E., Zhong, X., (2020). Augmentation of Bri2 molecular chaperone activity against amyloid-β reduces neurotoxicity in mouse hippocampus in vitro. *Commun. Biol.* **3**, 32.
50. Walsh, D.M., Thulin, E., Minogue, A.M., Gustavsson, N., Pang, E., Teplow, D.B., (2009). A facile method for expression and purification of the Alzheimer's disease-associated amyloid beta-peptide. *FEBS J.* **276**, 1266–1281.
51. Meisl, G., Kirkegaard, J.B., Arosio, P., Michaels, T.C.T., Vendruscolo, M., Dobson, C.M., (2016). Molecular mechanisms of protein aggregation from global fitting of kinetic models. *Nat. Protoc.* **11**, 252–272.
52. Ostendorp, T., Diez, J., Heizmann, C.W., Fritz, G., (2011). The crystal structures of human S100B in the zinc- and calcium-loaded state at three pH values reveal zinc ligand swapping. *Biochim. Biophys. Acta.* **1813**, 1083–1091.
53. van Zundert, G.C.P., Rodrigues, J.P.G.L.M., Trellet, M., Schmitz, C., Kastritis, P.L., Karaca, E., (2016). The HADDOCK2.2 Web Server: User-Friendly Integrative Modeling of Biomolecular Complexes. *J. Mol. Biol.* **428**, 720–725.